Atomic-Scale Geometry and Electronic Structure of Catalytically Important Pd/Au Alloys

Ashleigh E. Baber, Heather L. Tierney, and E. Charles H. Sykes*

Department of Chemistry, Tufts University, Medford, Massachusetts 02155-5813

ARTICLE

ABSTRACT Pd/Au bimetallic alloys catalyze many important reactions ranging from the synthesis of vinyl acetate and hydrogen peroxide to the oxidation of carbon monoxide and trimerization of acetylene. It is known that the atomic-scale geometry of these alloys can dramatically affect both their reactivity and selectivity. However, there is a distinct lack of experimental characterization and quantification of ligand and ensemble effects in this system. Low-temperature, ultrahigh vacuum scanning tunneling microscopy is used to investigate the atomic-scale geometry of Pd/Au{111} near-surface alloys and to spectroscopically probe their local electronic structure. The results reveal that the herringbone reconstruction of Au{111} provides entry sites for the incorporation of Pd atoms in the Au surface and that the degree of mixing is dictated by the surface temperature. At catalytically relevant temperatures the distribution of low coverages of Pd in the alloy is random, except for a lack of nearest neighbor pairs in both the surface and subsurface sites. Scanning tunneling spectroscopy is used to examine the electronic structure of the individual Pd atoms in surface and subsurface sites. This work reveals that in both surface and subsurface locations, Pd atoms display a very similar electronic structure to the surrounding Au atoms. However, individual surface and subsurface Pd atoms are depleted of charge in a very narrow region at the band edge of the Au surface state. d*I*/d*V* images of the phenomena demonstrate the spatial extent of this electronic perturbation.

KEYWORDS: metal alloys · palladium · gold · STM · electronic structure

Alloying metals is a very common way to modify their chemical and physical properties. In heterogeneous catalysis, both reaction activity and selectivity can be systematically altered *via* careful choice of bimetallic.[1−4] The complex interplay between elemental constituents that leads to superior catalytic performance is often discussed in terms of ligand and ensemble effects.[1,5] Ligand effects refer to the change in catalytic properties due to electronic interactions between the two elements of a bimetallic alloy. Ensemble effects refer to the spatial distribution of atomic sites that host reactants. Some reactions that require larger ensembles of reactive atoms to catalyze the transformation are halted when the active atom is monodispersed throughout an inert lattice.

Photoelectron spectroscopies have been used to investigate ligand effects in Pd/Au alloys with the aim of quantifying the charge transfer between the different atoms.[6−8] X-ray photoelectron spectroscopy (XPS) measures the binding energy of electrons in core levels of the surface atoms in a sample and can be used to quantify charge transfer between atoms or, in other words, determine oxidation states.[9] However, binding energy shifts in XPS occur not only from charge transfer, but other initial state effects like changes in coordination number, orbital rehybridization and also final state effects such as screening. Therefore, XPS alone is unsuitable for determining ligand effects in alloy systems.

Many experimentalists have studied Pd/Au surfaces and explained their catalytic performance in terms of geometric effects. Pd/Au alloys catalyze reactions as varied as the oxidation of CO[2,10] and crotyl alcohol,[11] the synthesis of vinyl acetate monomers (VAM)[3,4,12−14] and hydrogen peroxide,[5,15−17] the cyclotrimerization of acetylene to benzene,[7,18,19] the hydrogenation of polyunsaturated hydrocarbons,[20] and the electrooxidation of ethanol.[21−24] Goodman and co-workers have performed many surface studies of the alloy system and demonstrated that although Pd monomer pairs are most catalytically active for VAM synthesis on Au{100}, Pd monomers are most active on Au{111}.[3] Of particular relevance to the present study, it has been reported that annealing Pd/Au alloy films on Mo{110} results in a Au-enriched surface that contains only isolated Pd atoms.[13] Behm and co-workers have also shown that these same Pd monomers are catalytically active for CO oxidation, but that Pd dimers are needed for hydrogen adsorption.[2] Lambert and co-workers have examined the increase in catalytic activity and selectivity of Pd/Au alloys as a function of

*Address correspondence to charles.sykes@tufts.edu.

Received for review October 9, 2009 and accepted February 01, 2010.

Published online February 10, 2010.
10.1021/nn901390y

stoichiometery and temperature.[7,18,25] Tierney *et al.* demonstrated that individual, isolated Pd atoms in Cu{111} were active for H_2 dissociation and spillover, whereas Pd in Au{111} was not.[26] The Goodman and Behm groups have separately shown that even dilute amounts of Pd in Au{111} increase the catalytic ability of the substrate. Specifically, Pd monomers embedded in Au{111} are beneficial for VAM synthesis[3] and CO oxidation.[2] Therefore, elucidating the atomic-scale geometric and electronic structure of isolated Pd atoms in a Au host is crucial step for a more complete understanding of catalysis by Au/Pd alloys.

The aim of the current work is to elucidate the *local* geometry and electronic structure in the Pd/Au{111} system using scanning tunneling microscopy (STM) imaging and differential conductance (d*I*/d*V*) spectroscopy. These techniques allow the electronic structure of individual Pd atoms to be measured both in and under the Au surface. Small amounts of Pd were alloyed with Au{111} to mimic the structure of individual Pd monomers which are stable in the Au surface under catalytic conditions.[27] The fact that d*I*/d*V* spectra of both the Au and Pd atoms can be measured with the exact same STM tip allowed a direct comparison of the electronic structure of both sites without any spectral artifacts due to the electronic structure of the STM tip itself. Also, as d*I*/d*V* spectra represent the local density of states (LDOS) as a function of energy, the direction of charge transfer and the involved energy levels could be determined.

RESULTS AND DISCUSSION

The herringbone reconstruction of Au{111}, formally referred to as the 22x$\sqrt{3}$ reconstruction has been thoroughly studied using STM.[28,29] A large-scale atomically resolved image of a clean Au{111} surface is shown in Figure 1. The bright pairs of lines (soliton walls) arise due to extra Au atoms in the surface layer and they lie in three equivalent orientations 120° apart in order to reduce the surface strain evenly in all directions. Figure 1 also shows the locations of the alternating hexagonally close-packed (hcp) and face-centered cubic (fcc) domains on Au{111} that arise from packing of the surface Au atoms in either the hcp or fcc 3-fold hollow sites of the layer below.[28,29] The electronic structure of Au atoms differs in hcp and fcc domains, as previously reported by Crommie and others.[30,31] At every outer bulged and inner pinched elbow of the soliton wall pairs, an edge dislocation is present, where one atomic row terminates as shown in the inset of Figure 1.[25,28,29] The perturbed geometry and electron density of the under-coordinated Au atoms at edge dislocations allow these regions to act as preferential binding sites for adatoms or adsorbates.[32−34] To ensure that Pd atoms were indeed being studied, and not defects on the Au surface, particular attention was paid to the cleanliness of the bare Au{111} surface before depositing Pd. Clean

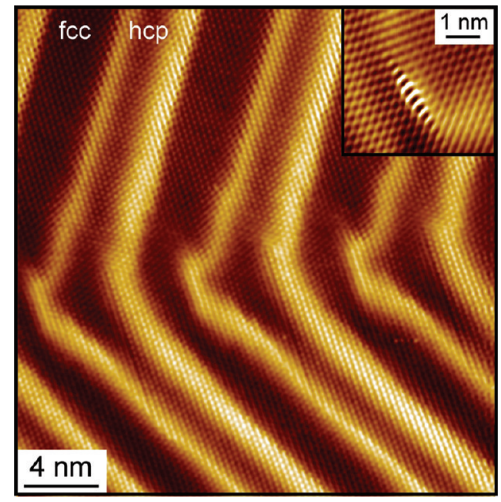

Figure 1. Large-scale atomic resolution STM image of clean Au{111} in which the herringbone reconstruction is visible. The pairs of bright lines are the soliton walls of the herringbone reconstruction which separate the hcp and fcc domains. A high resolution image of the atomic structure of an edge dislocation (present at the 120° bends of the soliton walls) is shown in the inset. Imaging conditions: −0.5 V, 1 nA, 80 K.

Au surfaces like that shown in Figure 1 could be routinely prepared with less than one defect per ~8000 surface atoms.

Figure 2 shows a representative area of Au{111} after physical vapor deposition of 0.005 monolayers (ML) of Pd atoms at a sample temperature of 380 K. At this deposition temperature the majority of the Pd atoms (imaged as protrusions surrounded by a dark "halo" as highlighted by the white arrows in Figure 2) were found to substitutionally alloy in the surface layers of the Au

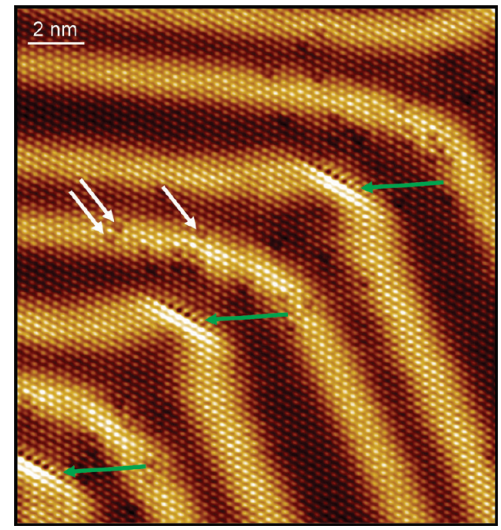

Figure 2. STM image of Au{111} after 0.005 ML Pd deposition at 380 K. The edge dislocations (green arrows) at the elbows of the herringbone reconstruction serve as entry sites for Pd atoms into the surface layer. The white arrows highlight three Pd atoms substituted into the surface layer. The majority of the Pd was found close to the elbows of the herringbone reconstruction, and the concentration of Pd atoms decreases dramatically further from the edge dislocations. Imaging conditions: 1.3 nA, 0.01 V, 7 K.

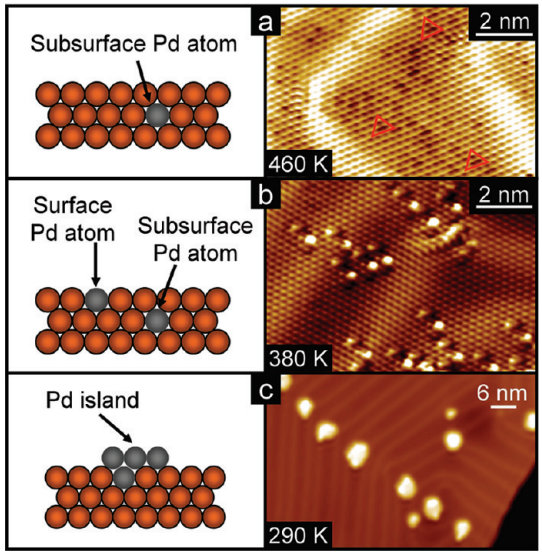

Figure 3. Temperature dependence of Pd's incorporation site in Au{111} (side view schematic and corresponding STM image). (a) After a 0.005 ML Pd deposition of 460 K, the majority of the Pd atoms reside in the subsurface layer and appear in the STM image as three-lobed depressions (highlighted by red triangles). Imaging conditions: 1.5 nA, −0.3 V, 7 K. (b) At a lower sample temperature (380 K) during 0.01 ML Pd deposition, Pd atoms are incorporated in the surface and subsurface layers. Subsurface Pd atoms appear as three-lobed features, whereas surface Pd atoms are protrusions. Imaging conditions: 0.5 nA, 0.1 V, 7 K. (c) Upon deposition at 290 K, Pd atoms place exchange with Au atoms at the edge dislocations and then serve as nucleation centers for the growth of monolayer high islands on top of the Au surface which are a Pd-rich mixture of Pd and Au. Imaging conditions: 0.005 ML Pd, 0.3 nA, 0.3 V, 80 K.

sample in the vicinity of the edge dislocations (green arrows in Figure 2). The reduced coordination and bond strength of the Au atoms at edge dislocations allowed for the preferential place exchange of Pd atoms to occur. This result is in agreement with the predictions made by Behm and co-workers due to the higher surface free energy and heat of sublimation of Pd in comparison to Au.[35] The vast majority of the Pd atoms were found to alloy in the immediate vicinity of the edge dislocations. Varga and Schmid explained the origin of chemical contrast in different alloy systems in terms of both intrinsic differences in electronic/geometric structure and tip−sample interaction.[36] The Besenbacher and Goodman groups have recently performed high-resolution STM studies on Cu/Pt and Au/Pd alloys, respectively.[4,37] Besenbacher and co-workers studied the alloying of Pt with Au{111} and found that Pt occupied the areas around edge dislocations and step edges of the Au surface.[38] Goodman and co-workers found that even though Pd atoms have a smaller diameter than Au (Pd = 0.275 nm, Au = 0.288 nm), individual surface Pd atoms in Au/Pd{100} imaged as protrusions with apparent height between 0.01 and 0.06 nm.[4]

Depending on the sample temperature during alloying, Pd atoms were found to reside in the subsurface and surface layers of Au{111} as well as on the surface as adatom islands, as shown by STM images and schematics in Figure 3. High surface temperature depositions yielded stable alloys with Pd fully coordinated below the surface (subsurface Pd), intermediate temperatures produced mainly surface Pd atoms, and lower temperature depositions resulted in a metastable system with Pd-rich islands on top of the surface. After a Pd deposition at an average sample temperature of 460 K, most of the Pd atoms were located in the subsurface region and imaged as three-lobed depressions, as seen in Figure 3a. After annealing a 5 ML Au/Pd{111} sample, Tysoe and co-workers observed that the surface layer was Au-enriched while the second layer was an intermediate between the top and bulk layer compositions.[39] Deposition at a sample temperature of 380 K led to the majority of Pd atoms being alloyed substitutionally into the surface layer in the vicinity of the edge dislocations at the elbows of the herringbone reconstruction. The surface Pd atoms appeared in STM images as both depressions and protrusions in Au{111} depending on the imaging conditions.[2] At the conditions used to record Figure 3b, the surface Pd atoms appeared as protrusions. Finally, after a deposition at a lower sample temperature of 290 K, adatom island formation occurred in which Pd atoms were present in the form of islands on top of the Au surface. These results reflect the higher surface free energy of Pd compared to Au (surface free energy: Au = 1.63 J m^{-2}; Pd = 2.05 J m^{-2}).[40] At lower deposition temperatures place-exchanged Pd atoms at the elbows acted as nucleation sites for the growth of adatom islands as seen in Figure 3c and in the Supporting Information.[41,42] The islands grew toward the fcc areas at bulged elbows, as previously observed by Lambert and co-workers.[25]

It is important to note that a previous study of this system reported atomic-scale depressions on the surface after Pd deposition at room temperature and assigned them as individual Pd atoms residing in fcc 3-fold hollow sites.[43] The fact that these features could be imaged at 300 K for a number of minutes precludes them from being isolated atoms on the surface. In fact, isolated metal atoms on {111} facets of noble metal surfaces have fairly low diffusion barriers, typically less than 100 meV. For example the Al/Au{111} system has an experimentally measured barrier of 30 ± 5 meV[44] and Ag/Ag{111} has a barrier of 97 ± 10 meV.[45] Assuming a modest attempt frequency of 1×10^{13} and a diffusion barrier of 100 meV, the rate of diffusing metal atoms across a Au{111} surface at room temperature is $\sim 2 \times 10^{11}$ s^{-1}. Therefore it would be impossible to detect isolated Pd atoms diffusing on Au{111} at 300 K using STM imaging. We suggest that the depressions reported in the aforementioned study are in fact either surface Pd atoms imaged with a different tip state, subsurface Pd atoms, or impurities.

It is evident from Figures 2 and 3 that there is no long-range order of surface or subsurface Pd atoms in

Au{111}. The only order that exists is a distinct lack of nearest neighbor Pd atoms.[46] This apparent repulsion between nearest neighbor Pd atoms stems from stronger heteroatom Pd−Au bonds as compared to weaker Au−Au and Pd−Pd bonds.[47] The ramification of this nearest neighbor repulsion between Pd atoms is that in any dilute alloy surface Pd atoms will be surrounded by six Au atoms with the nearest possible Pd atom $\sqrt{3}d$ away. We show here that this effect is relevant over a fairly wide range of temperatures (290−500 K) at which Au/Pd catalysts typically operate.[3,5,7] Therefore, elucidation of the geometric, electronic, and reactive properties of Pd atoms locally coordinated by Au is a crucial step toward understanding the fundamental workings of these systems.

Now that we have quantified the atomic-scale geometry (ensemble effects) of the Pd/Au{111} system we will focus on using the spectroscopy capabilities of the low-temperature STM to measure the electronic structure (ligand effects) of the Pd/Au system. In terms of electronic structure, the d-band model uses the energy of the d-band center with respect to the Fermi level as a predictor of adsorbate binding strength and therefore reactivity.[48−51] The closer the d-band to the Fermi level, the stronger an adsorbate binds. In alloy systems variations in elemental composition, and hence the d-band center, determine adsorbate binding and reactivity. In general, without the use of theoretical modeling it has been difficult to separate ligand and ensemble effects. This is because varying the composition of the elements in a surface simultaneously affects both the geometry and the electronic structure of the alloy. Norskov and co-workers used DFT calculations to decouple ligand and ensemble effects in the adsorption of small molecules on Au/Pd{111} alloy surfaces and found that in the case of adsorption, the ensemble effect dominates.[1,52] In contrast, a recent theoretical investigation of CO oxidation highlighted the importance of the Au induced ligand effect in Pd−Au alloys.[53]

In this paper, the ligand effect was investigated using d*I*/d*V* point spectroscopy, in which the LDOS of individual Pd atoms both in and under the surface were recorded 1 eV above and below the Fermi level (E_F). Individual electronic spectra (either *I vs V* or d*I*/d*V vs V*) recorded using any scanning probe technique have the inherent problem that the spectra contain contributions from the electronic structure of the probe tip itself as well as the sample. For example, the d*I*/d*V* spectra of the fcc and hcp regions of clean Au{111} presented in Figures 4c and 5a are of identical Au samples but recorded with different STM tips. It is obvious from inspection of both sets of spectra that, while the surface state appears at the same energy, the background d*I*/d*V* intensity is markedly different. To eliminate such tip artifacts in our quantification of d*I*/d*V* data we used the same tip to record spectra over bare Au surface atoms and Pd atoms both in and under the Au surface (Figure 4 and 5). Changes in the STM tip state were very noticeable not only in the topographic images (which were taken concurrently with d*I*/d*V* spectra measurements), but also large spikes were observed in d*I*/d*V* spectra when a tip change occurred due to saturation of the signal from the lock-in amplifier. To ensure that all data was recorded with the same STM tip state, d*I*/d*V* spectra were always taken multiple times alternating between Pd and Au atoms. If the tip had changed within the set of measurements, then the Pd spectra at the beginning and end of the set would differ and the data set would be discarded.

The fact that d*I*/d*V* spectra of both the Au{111} surface atoms and inserted Pd atoms could be measured with exactly the same tip allowed a direct comparison of the electronic structure of both atomic sites with subnanometer resolution without tip artifacts. Spectra were taken of surface and subsurface Pd atoms in both the fcc and hcp regions of the Au{111} crystal and compared to the spectra of Au atoms in the respective areas. The first point to address is the reproducibility of individual, single-sweep d*I*/d*V* point spectra. Figure 4 panels a and b show five individual d*I*/d*V* curves for surface Pd atoms in the hcp and fcc regions of the Au herringbone reconstruction and the average of all five. It is important to note that while we present d*I*/d*V* spectra that are the average of five individual spectra in this paper, the individual single-sweep curves all exhibit

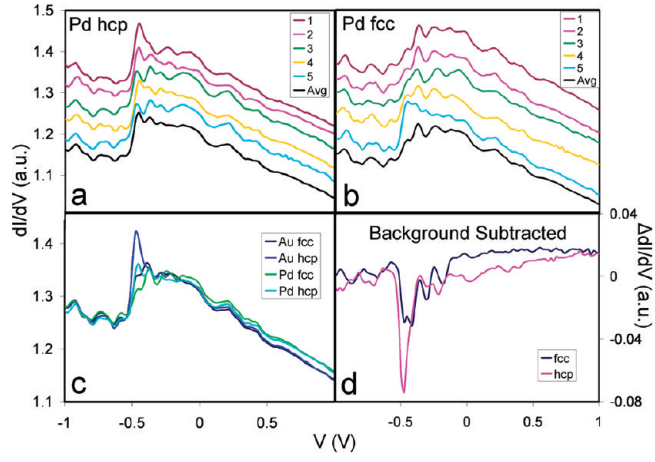

Figure 4. Electronic spectra of individual surface Pd atoms in a Pd/Au alloy. (a) Five individual, single-sweep d*I*/d*V* spectra for a surface Pd atom residing in the hcp region of the Au{111} surface. The average (avg) d*I*/d*V* curve of the five single-sweep spectra is shown in black. The spectra have been offset in the *y*-axis for clarity. (b) Average (black line) and five single-sweep measurements for individual surface Pd atoms in the fcc region of the herringbone reconstruction. (c) d*I*/d*V* spectra for surface Au and Pd atoms in both hcp and fcc regions. (d) Background subtraction spectra of Pd atoms in the respective regions. Dips in the spectra in Figure 4d are seen for both Pd atoms in hcp and fcc regions at ~0.45 eV below the Fermi energy.

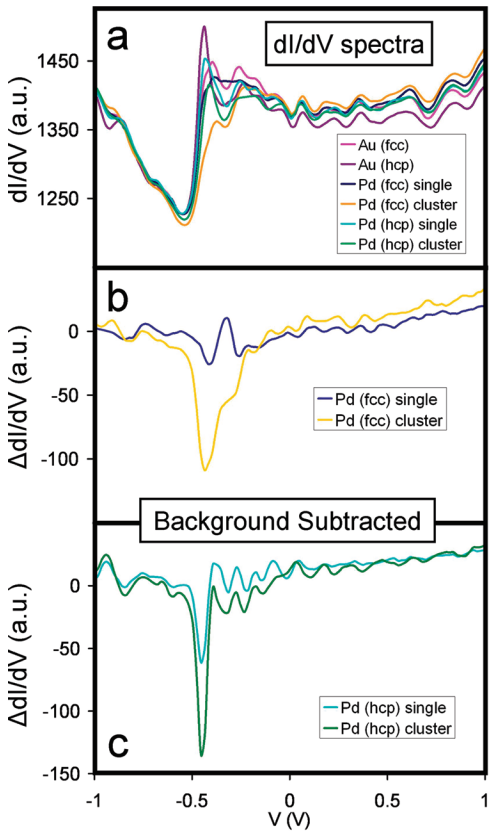

Figure 5. Electronic spectra of subsurface Pd atoms and clusters in a Pd/Au alloy. (a) d*I*/d*V* spectra taken over each of the following atoms: subsurface Pd atoms, either individually or in a cluster of subsurface Pd atoms and Au atoms in the fcc and hcp domains of the Au herringbone reconstruction. (b and c) Spectra in which the relevant areas of the bare Au{111} background electron density have been subtracted from the Pd spectra for fcc and hcp regions of the surface, respectively. Panels b and c show that a single subsurface Pd atom has a relatively small effect on the surface electron density in fcc regions and a larger effect in hcp areas. However, the spectra of Pd atoms at the center of clusters of subsurface Pd atoms show a much greater quenching of the electron density of the Au{111} surface than do isolated subsurface Pd atoms.

the same features in a reproducible manner. The reason for using five curve averages was that the charge transfer between atoms could be quantified more accurately. The d*I*/d*V* spectra for Au atoms in the fcc and hcp regions of the Au{111} surface were in good agreement with those recorded by Crommie and coworkers.[30] Figure 4c shows average d*I*/d*V* spectra of both surface Pd and Au atoms in both fcc and hcp areas of the Au{111} surface. At first glance all of the spectra looked almost identical. Therefore, to first approximation, isolated surface Pd atoms are electronically identical to their Au host. However, as all of these spectra were taken using the same STM tip, the Au background could be subtracted from the Pd spectra to reveal subtle differences in the LDOS of the Au and Pd atoms as seen in Figure 4d.

The major difference in the electronic structure of surface Pd atoms and Au atoms lies at an energy very close to the Au{111} surface state band edge (*ca.* −0.45 eV[30]). The surface Pd atoms quench a narrow region of this electron density and are thus themselves depleted of electron density at this energy. Figure 4d reveals that Pd atoms in the hcp area are more electron deficient with respect to their neighboring Au atoms than Pd atoms in the fcc area.

Figure 5 shows d*I*/d*V* spectra of subsurface Pd atoms in the fcc and hcp regions of the Au{111} surface. Spectra were taken over both isolated Pd subsurface atoms and subsurface Pd atoms in "clusters" with 4−8 other subsurface Pd atoms within an area of ∼1.6 nm^2. Figures 5 panels b and c show subsurface Pd spectra in which the Au background has been subtracted in order to demonstrate how the presence of subsurface Pd atoms affected the electron density of the Au{111} surface above it. It is evident from these spectra that both the surface and subsurface Pd atoms quench the same region at the surface state band edge of the Au{111} as do surface Pd atoms. Comparing Figure 5 panels b and c revealed that, just like surface Pd atoms, subsurface Pd atoms in hcp areas quench the surface state to a greater degree than those in fcc areas. Clusters of subsurface Pd atoms depleted the surface electron density to a greater extent than individual atoms. The charge transfer from the Pd atoms to the Au substrate was quantified by integrating the region of the d*I*/d*V* spectra that corresponded to the surface state of Au{111}. Then, by referencing the Wigner−Seitz radius of Au (8.9 Å), the original electron density contained in the surface state of Au{111} was calculated. Quantifying the difference between the d*I*/d*V* spectra of individual Au and Pd atoms allowed the depletion of electron density at the Pd atom positions, and therefore the charge transfer between Pd and Au, to be quantified. There was a slightly larger charge transfer from surface Pd atoms to Au in the hcp regions (0.0007 e$^-$) as compared to the fcc regions (0.0004 e$^-$). Clusters of subsurface Pd atoms transfer a greater number of electrons to Au as compared to single subsurface Pd atoms in both fcc and hcp regions (0.001 e$^-$ and 0.0002 e$^-$, respectively, in fcc regions; 0.008 e$^-$ and 0.0006 e$^-$ in hcp regions). The hcp sites in Au{111} are more electron-rich than fcc sites at an energy of −0.45 eV as shown by Crommie's group.[30] Therefore, greater charge transfer occurs in hcp regions due to the larger amount of electron density available to quench at this energy.

After measuring the magnitude of the charge transfer, its spatial effect was investigated using d*I*/d*V* imaging which outputs the spatial variation of the electron density of the surface as a function of the energy. In this way the size of the area depleted of charge around the Pd atoms could be measured. Figure 6a is an atomically resolved topographic image of two surface Pd atoms that appear as protrusions. The d*I*/d*V* image in Figure 6b was obtained at a sample bias of −0.45 V, which corresponded to the energy of the charge depleted re-

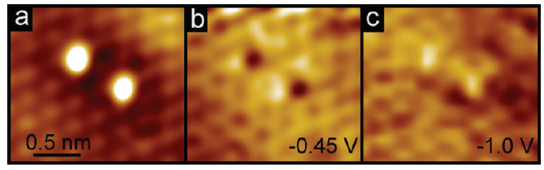

Figure 6. Topographic and d*I*/d*V* images of surface Pd atoms in Au{111} at various energies. Figure 6a is an atomically resolved topographic STM image in which two surface Pd atoms appear as protrusions. Imaging conditions: 2 nA, −0.5 V. Figure 6b shows a d*I*/d*V* image of the same area of the surface shown in 6a at recorded at a sample bias of −0.45 V, corresponding to the energy at which d*I*/d*V* spectra show differences for Pd and Au atoms. This d*I*/d*V* image reveals that the Pd atoms are indeed depleted of charge at this energy and that the charge depletion is spatially localized on the atom itself. In Figure 6c the d*I*/d*V* image was recorded at a sample bias of −1.0 V, corresponding to an energy at which the Pd and Au atoms are electronically very similar and the Pd atoms are almost indistinguishable from the Au host.

gion that arises from the presence of surface Pd (Figure 4). In the d*I*/d*V* map the Pd atoms appeared as localized depressions the same size as the Pd atoms themselves. This indicates that the depletion of charge affected an area no larger than the isolated Pd atom itself (~0.28 nm in diameter). In Figure 6c, the d*I*/d*V* image was recorded at −1 V, corresponding to an energy at which the electron density of Pd and Au spectra are the same. In this case, the Pd atoms were barely visible in the d*I*/d*V* map, verifying that the Pd and Au atoms were nearly electronically identical at this energy, as indicated by the d*I*/d*V* point spectroscopy.

To put these results in context, the effect of surface defects and adatoms on the electronic structure of surfaces has been reported by several groups.[54−57] Using d*I*/d*V* spectroscopy, Eigler and co-workers revealed that monatomic step edges quenched the entire Cu{111} surface state over an energy range ~1 eV.[55] Similarly, Weiss and co-workers found that in the vicinity of Br adatom islands on Cu{111} the entire surface state was quenched.[56] In both studies the effect was explained by the strong electron scattering produced by defects and adsorbates. Pd has been observed to quench a narrow region of the surface state of another noble metal, Cu{111}, as well.[58] In the present study the surface state quenching was very localized spatially, as well as in energy with a FWHM of <0.05 eV.

To investigate the origin of the charge transfer effects observed here larger scale d*I*/d*V* imaging was performed to examine the effect of Pd atoms on the surface state electrons. The wavelike nature of the electronic surface state was directly visualized in the regions of any defects that acted as scattering centers. Figure 7 shows topographic and d*I*/d*V* images for both bare Au{111} and the 0.005 ML Pd/Au{111} surface. The depression near the center of the clean Au{111} image originated from residual subsurface impurities that weakly perturbed the surface electronic state density but did not contribute to scattering. On the bare

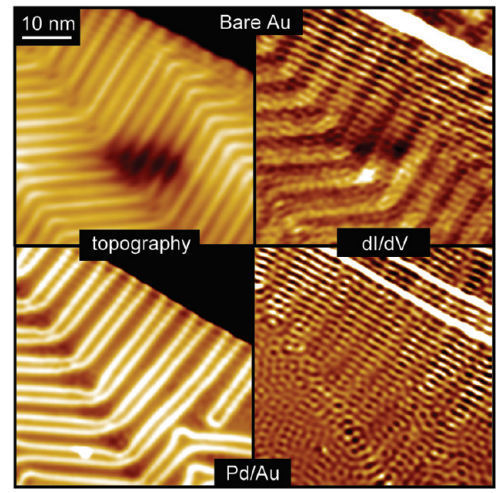

Figure 7. Topographic and d*I*/d*V* images of bare Au{111} and 0.005 ML Pd/Au{111}. The images in the left panels are topographic images of bare Au and Pd/Au{111}. Monatomic Au step edges are present in the upper right-hand corner of each image. The elbows of the alloy surface contain the majority of the Pd atoms. The images in the right panels are d*I*/d*V* images which show the LDOS of the surface while removing all topographic features. It is seen that while the step edge is the predominant scatterer on bare Au{111}, Pd sites scatter strongly in the alloy surface. Imaging conditions: 1.5 nA, 0.1 V, 7 K.

Au{111} surface it is evident in the d*I*/d*V* images that the step edge in the upper right-hand corner of the image acts as the predominant scattering site for the surface-state electrons. Importantly, the d*I*/d*V* images of bare Au{111} reveal that the elbows of the herringbone reconstruction do not contribute significantly to electron scattering. However, inspection of the d*I*/d*V* image in the bottom right panel of Figure 7 shows that scattering occurs in the Pd/Au alloy surface at the elbows of the herringbone reconstruction where the Pd atoms reside. The scattering which appears as a diagonal line (top left to bottom right) tracks the elbows of the herringbone reconstruction and has a similar amplitude as the scattering observed at step edges. These results reveal that, unlike earlier work in which Pd layers on Au{111} were found to shift the surface state electrons to longer wavelengths, addition of small amounts of Pd atoms in the surface and subsurface layers of Au{111} act as scattering centers for the surface state electrons but do not change their wavelength.[59,60] This demonstrates that the presence of a small amount of Pd does not quench the surface state as might be expected for impurities that perturb the flat 2D surface state potential but leads to substantial scattering effects of similar magnitude to step-edge defects. While this scattering is a possible mechanism by which Pd atoms are depleted of charge, our data reveals that electron scattering occurs over a wide energy range (~0.7 eV) but that the Pd atoms are depleted of charge in a much narrower range of energies (~0.05 eV) and that this charge depletion is very localized in space (~0.3

nm). This indicates that electron scattering is most likely not the cause of the charge transfer effect. We suggest that further modeling work is needed to explain the origin of the effect we observe experimentally.

CONCLUSIONS

Gold's ability to temper palladium's reactivity and tune its selectivity makes the Pd/Au alloy a crucial component of a variety of industrially important catalysts. Different compositions lead to a complex geometry and associated electronic structure, both of which have been shown to have dramatic effects on the alloy's chemistry. This study was aimed at elucidating the atomic-scale structure of a Pd/Au{111} model system and measuring subtle local electronic differences between the constituent atoms. We found that at the dilute limit the most stable configuration consisted of isolated Pd atoms beneath the Au surface. Pd deposition at lower sample temperatures yielded isolated monomers in the surface layer and room temperature alloying resulted in the growth of arrays of Pd islands. We discovered that isolated Pd atoms both in and under the Au surface had an electronic structure almost identical to their host metal, except for a very small charge depletion from the Pd near the peak in the Au surface state. d*I*/d*V* imaging revealed that this effect was entirely localized on the Pd atom itself and that while the Pd "defects" do not quench the surface state the isolated Pd atoms serve as scattering centers. While the measurements were conducted at low temperatures, the actual geometric arrangements of atoms studied are similar to those in Pd/Au alloys at catalytically relevant temperatures. At high temperatures (>400 K) Pd diffuses to more stable sites in the subsurface and bulk of Au. However, in the presence of reactive species Pd will actually segregate back to the surface as both single atoms and clusters. Therefore, our study of the geometric and electronic properties of both surface and subsurface Pd has relevance to real catalytic Pd/Au alloy particles which will contain similar ensembles of Pd atoms. Future studies are aimed at extending the energy of these measurements and making comparisons to theory.

EXPERIMENTAL SECTION

Experiments were performed in an Omicron Nano-Technology LT-UHV STM.[61] The very high stability of the microscope at 7 K allows imaging to occur in a particular area of the surface for many hours with minimal thermal drift. A Princeton Scientific Corporation Au single crystal surface was prepared by many consecutive Ar^+ sputter (1 keV/12 μA) and anneal (1000 K) cycles. A home-built Pd source (0.05 mm Pd wire doubly wrapped around a 0.25 mm W wire) was used to deposit Pd directly onto the Au{111} sample at a variety of sample temperatures in the preparation chamber. All of the scanning conditions are reported for the sample voltage. Sample temperatures are accurate to within ±10 K. Differential conductance (d*I*/d*V*) images/spectra were acquired using a lock-in amplifier by modulating the bias voltage with a 1 kHz ac 12 mV amplitude signal and recorded with a 10/300 ms time constant, respectively, at a sample and tip temperature of 7 K.

Acknowledgment. We thank the NSF (Grant No. 0828666), the Beckman Foundation and Research Corporation for support of this research. A.E.B. and H.L.T. acknowledge the U.S. Department of Education for GAANN fellowships. E.C.H.S. is grateful to the Usen family for their support. The authors thank Eric Heller and Don Eigler for useful discussions about the data.

Supporting Information Available: Additional STM images are available which show the distortion of the herringbone reconstruction due to surface alloying and evidence for the occurrence of place-exchange prior to island nucleation during Pd deposition on Au{111}. This material is available free of charge *via* the Internet at http://pubs.acs.org.

REFERENCES AND NOTES

1. Liu, P.; Norskov, J. K. Ligand and Ensemble Effects in Adsorption on Alloy Surfaces. *Phys. Chem. Chem. Phys.* **2001**, *3*, 3814–3818.
2. Maroun, F.; Ozanam, F.; Magnussen, O. M.; Behm, R. J. The Role of Atomic Ensembles in the Reactivity of Bimetallic Electrocatalysts. *Science* **2001**, *293*, 1811–1814.
3. Chen, M. S.; Kumar, D.; Yi, C. W.; Goodman, D. W. The Promotional Effect of Gold in Catalysis by Palladium−Gold. *Science* **2005**, *310*, 291–293.
4. Han, P.; Axnanda, S.; Lyubinetsky, I.; Goodman, D. W. Atomic-Scale Assembly of a Heterogeneous Catalytic Site. *J. Am. Chem. Soc.* **2007**, *129*, 14355–14361.
5. Landon, P.; Collier, P. J.; Carley, A. F.; Chadwick, D.; Papworth, A. J.; Burrows, A.; Kiely, C. J.; Hutchings, G. J. Direct Synthesis of Hydrogen Peroxide from H_2 and O_2 using Pd and Au Catalysts. *Phys. Chem. Chem. Phys.* **2003**, *5*, 1917–1923.
6. Koel, B. E.; Sellidj, A.; Paffett, M. T. Ultrathin Films of Pd on Au(111)—Evidence for Surface Alloy Formation. *Phys. Rev. B* **1992**, *46*, 7846–7856.
7. Baddeley, C. J.; Ormerod, R. M.; Stephenson, A. W.; Lambert, R. M. Surface-Structure and Reactivity in the Cyclization of Acetylene to Benzene with Pd Overlayers and Pd/Au Surface Alloys on Au(111). *J. Phys. Chem.* **1995**, *99*, 5146–5151.
8. Li, Z. J.; Gao, F.; Wang, Y. L.; Calaza, F.; Burkholder, L.; Tysoe, W. T. Formation and Characterization of Au/Pd Surface Alloys on Pd(111). *Surf. Sci.* **2007**, *601*, 1898–1908.
9. Kulprathipanja, A.; Alptekin, G. O.; Falconer, J. L.; Way, J. D. Pd and Pd−Cu Membranes: Inhibition of H_2 Permeation by H_2S. *J. Membr. Sci.* **2005**, *254*, 49–62.
10. Gao, F.; Wang, Y.; Goodman, D. W. CO Oxidation over AuPd(100) from Ultrahigh Vacuum to Near-Atmospheric Pressures: The Critical Role of Contiguous Pd Atoms. *J. Am. Chem. Soc.* **2009**, *131*, 5734–5735.
11. Lee, A. F.; Hackett, S. F. J.; Hutchings, G. J.; Lizzit, S.; Naughton, J.; Wilson, K. *In Situ* X-ray Studies of Crotyl Alcohol Selective Oxidation over Au/Pd(1 1 1) Surface Alloys. *Catal. Today* **2009**, *145*, 251–257.
12. Kumar, D.; Chen, M. S.; Goodman, D. W. Synthesis of Vinyl Acetate on Pd-Based Catalysts. *Catal. Today* **2007**, *123*, 77–85.
13. Wei, T.; Wang, J.; Goodman, D. W. Characterization and Chemical Properties of Pd−Au Alloy Surfaces. *J. Phys. Chem. C* **2007**, *111*, 8781–8788.
14. García-Mota, M.; López, N. Template Effects in Vinyl Acetate Synthesis on PdAu Surface Alloys: A Density Functional Theory Study. *J. Am. Chem. Soc.* **2008**, *130*, 14406–14407.
15. Landon, P.; Collier, P. J.; Papworth, A. J.; Kiely, C. J.;

Hutchings, G. J. Direct Formation of Hydrogen Peroxide from H_2/O_2 Using a Gold Catalyst. *Chem. Commun.* **2002**, 2058–2059.
16. Han, Y. F.; Zhong, Z. Y.; Ramesh, K.; Chen, F. X.; Chen, L. W.; White, T.; Tay, Q. L.; Yaakub, S. N.; Wang, Z. Au Promotional Effects on the Synthesis of H_2O_2 directly from H_2 and O_2 on supported Pd−Au Alloy Catalysts. *J. Phys. Chem. C* **2007**, *111*, 8410–8413.
17. Edwards, J. K.; Solsona, B.; N, E. N.; Carley, A. F.; Herzing, A. A.; Kiely, C. J.; Hutchings, G. J. Switching Off Hydrogen Peroxide Hydrogenation in the Direct Synthesis Process. *Science* **2009**, *323*, 1037–1041.
18. Baddeley, C. J.; Tikhov, M.; Hardacre, C.; Lomas, J. R.; Lambert, R. M. Ensemble Effects in the Coupling of Acetylene to Benzene on a Bimetallic Surface: A Study with Pd{111}/Au. *J. Phys. Chem.* **1996**, *100*, 2189–2194.
19. Lee, A. F.; Baddeley, C. J.; Hardacre, C.; Ormerod, R. M.; Lambert, R. M. Structural and Catalytic Properties of Novel Au/Pd Bimetallic Colloid Particles: EXAFS, XRD, and Acetylene Coupling. *J. Phys. Chem.* **1995**, *99*, 6096–6102.
20. Redjala, T.; Remita, H.; Apostolescu, G.; Mostafavi, M.; Thomazeau, C.; Uzio, D. Bimetallic Au−Pd and Ag−Pd Clusters Synthesised by Gamma or Electron Beam Radiolysis and Study of the Reactivity/Structure Relationships in the Selective Hydrogenation of Buta-1,3-diene. *Oil Gas Sci. Technol. Rev. Inst. Fr. Pet.* **2006**, *61*, 789–797.
21. He, Q. G.; Chen, W.; Mukerjee, S.; Chen, S. W.; Laufek, F. Carbon-supported PdM (M = Au and Sn) nanocatalysts for the electrooxidation of ethanol in high pH media. *J. Power Sources* **2009**, *187*, 298–304.
22. Ksar, F.; Ramos, L.; Keita, B.; Nadjo, L.; Beaunier, P.; Remita, H. Bimetallic Palladium−Gold Nanostructures: Application in Ethanol Oxidation. *Chem. Mater.* **2009**, *21*, 3677–3683.
23. Liu, Z. L.; Zhao, B.; Guo, C. L.; Sun, Y. J.; Xu, F. G.; Yang, H. B.; Li, Z. Novel Hybrid Electrocatalyst with Enhanced Performance in Alkaline Media: Hollow Au/Pd Core/Shell Nanostructures with a Raspberry Surface. *J. Phys. Chem. C* **2009**, *113*, 16766–16771.
24. Zhu, L. D.; Zhao, T. S.; Xu, J. B.; Liang, Z. X. Preparation and Characterization of Carbon-Supported Submonolayer Palladium Decorated Gold Nanoparticles for the Electro-oxidation of Ethanol in Alkaline Media. *J. Power Sources* **2009**, *187*, 80–84.
25. Stephenson, A. W.; Baddeley, C. J.; Tikhov, M. S.; Lambert, R. M. Nucleation and Growth of Catalytically Active Pd Islands on Au(111)-22x$\sqrt{3}$ Studied by Scanning Tunnelling Microscopy. *Surf. Sci.* **1998**, *398*, 172–183.
26. Tierney, H. L.; Baber, A. E.; Kitchin, J. R.; Sykes, E. C. H. Hydrogen Dissociation and Spillover on Individual Isolated Palladium Atoms. *Phys. Rev. Lett.* **2009**, *103*, 246102.
27. Wang, D.; Villa, A.; Porta, F.; Prati, L.; Su, D. Bimetallic Gold/Palladium Catalysts: Correlation between Nanostructure and Synergistic Effects. *J. Phys. Chem. C* **2008**, *112*, 8617–8622.
28. Barth, J. V.; Brune, H.; Ertl, G.; Behm, R. J. Scanning Tunneling Microscopy Observations on the Reconstructed Au(111) Surface—Atomic-Structure, Long-Range Superstructure, Rotational Domains, and Surface-Defects. *Phys. Rev. B* **1990**, *42*, 9307–9318.
29. Woll, C.; Chiang, S.; Wilson, R. J.; Lippel, P. H. Determination of Atom Positions at Stacking-Fault Dislocations on Au(111) by Scanning Tunneling Microscopy. *Phys. Rev. B* **1989**, *39*, 7988–7991.
30. Chen, W.; Madhavan, V.; Jamneala, T.; Crommie, M. F. Scanning Tunneling Microscopy Observation of an Electronic Superlattice at the Surface of Clean Gold. *Phys. Rev. Lett.* **1998**, *80*, 1469–1472.
31. Burgi, L.; Brune, H.; Kern, K. Imaging of Electron Potential Landscapes on Au(111). *Phys. Rev. Lett.* **2002**, *89*, 1768011–1768014.
32. Chambliss, D. D.; Wilson, R. J.; Chiang, S. Ordered Nucleation of Ni and Au Islands on Au(111) Studied by Scanning Tunneling Microscopy. *J. Vac. Sci. Technol. B* **1991**, *9*, 933–937.
33. Voigtlander, B.; Meyer, G.; Amer, N. M. Epitaxial-Growth of Thin Magnetic Cobalt Films on Au(111) Studied by Scanning Tunneling Microscopy. *Phys. Rev. B* **1991**, *44*, 10354–10357.
34. Stroscio, J. A.; Eigler, D. M. Atomic and Molecular Manipulation with the Scanning Tunneling Microscope. *Science* **1991**, *254*, 1319–1326.
35. Meyer, J. A.; Baikie, I. D.; Kopatzki, E.; Behm, R. J. Preferential Island Nucleation at the Elbows of the Au(111) Herringbone Reconstruction through Place Exchange. *Surf. Sci.* **1996**, *365*, L647–L651.
36. Varga, P.; Schmid, M. Chemical Discrimination on Atomic Level by STM. *Appl. Surf. Sci.* **1999**, *141*, 287–293.
37. Knudsen, J.; Nilekar, A. U.; Vang, R. T.; Schnadt, J.; Kunkes, E. L.; Dumesic, J. A.; Mavrikakis, M.; Besenbacher, F. A Cu/Pt Near-Surface Alloy for Water−Gas Shift Catalysis. *J. Am. Chem. Soc.* **2007**, *129*, 6485–6490.
38. Pedersen, M. O.; Helveg, S.; Ruban, A.; Stensgaard, I.; Laegsgaard, E.; Norskov, J. K.; Besenbacher, F. How a Gold Substrate Can Increase the Reactivity of a Pt Overlayer. *Surf. Sci.* **1999**, *426*, 395–409.
39. Li, Z. J.; Furlong, O.; Calaza, F.; Burkholder, L.; Poon, H. C.; Saldin, D.; Tysoe, W. T. Surface Segregation of Gold for Au/Pd(111) Alloys Measured by Low-Energy Electron Diffraction and Low-Energy Ion Scattering. *Surf. Sci.* **2008**, *602*, 1084–1091.
40. Mezey, L. Z.; Giber, J. The Surface Free-Energies of Solid Chemical-Elements—Calculation from Internal Free Enthalpies of Atomization. *Jpn. J. Appl. Phys., Part 1* **1982**, *21*, 1569–1571.
41. Meyer, J. A.; Behm, R. J. Place-Exchange as a Mechanism for Adlayer Island Nucleation during Epitaxial Growth and Resulting Scaling Behavior. *Surf. Sci.* **1995**, *322*, L275–L280.
42. Chambliss, D. D.; Wilson, R. J.; Chiang, S. Nucleation of Ordered Ni Island Arrays on Au(111) by Surface-Lattice Dislocations. *Phys. Rev. Lett.* **1991**, *66*, 1721–1724.
43. Casari, C. S.; Foglio, S.; Siviero, F.; Bassi, A. L.; Passoni, M.; Bottani, C. E. Direct Observation of the Basic Mechanisms of Pd Island Nucleation on Au(111). *Phys. Rev. B.* **2009**, *79*, 1954021–1954029.
44. Fischer, B.; Brune, H.; Barth, J. V.; Fricke, A.; Kern, K. Nucleation Kinetics on Inhomogeneous Substrates: Al/Au(111). *Phys. Rev. Lett.* **1999**, *82*, 1732–1735.
45. Brune, H.; Bromann, K.; Roder, H.; Kern, K.; Jacobsen, J.; Stoltze, P.; Jacobsen, K.; Norskov, J. Effect of Strain on Surface-Diffusion and Nucleation. *Phys. Rev. B* **1995**, *52*, 14380–14383.
46. Boscoboinik, J. A.; Plaisance, C.; Neurock, M.; Tysoe, W. T. Monte Carlo and Density Functional Theory Analysis of the Distribution of Gold and Palladium Atoms on Au/Pd(111) Alloys. *Phys. Rev. B* **2008**, *77*, 0454221−0454226.
47. Yuan, D. W.; Gong, X. G.; Wu, R. Q. Atomic Configurations of Pd Atoms in PdAu(111) Bimetallic Surfaces Investigated Using the First-Principles Pseudopotential Plane Wave Approach. *Phys. Rev. B* **2007**, *75*, 0854281−0854285.
48. Bligaard, T.; Norskov, J. K. Ligand Effects in Heterogeneous Catalysis and Electrochemistry. *Electrochim. Acta* **2007**, *52*, 5512–5516.
49. Hammer, B.; Norskov, J. K. Theoretical Surface Science and Catalysis—Calculations and Concepts. *Adv. Catal.* **2000**, *45*, 71–129.
50. Nilsson, A.; Pettersson, L. G. M.; Hammer, B.; Bligaard, T.; Christensen, C. H.; Norskov, J. K. The Electronic Structure Effect in Heterogeneous Catalysis. *Catal. Lett.* **2005**, *100*, 111–114.
51. Norskov, J. K.; Bligaard, T.; Logadottir, A.; Bahn, S.; Hansen, L. B.; Bollinger, M.; Bengaard, H.; Hammer, B.; Sljivancanin, Z.; Mavrikakis, M.; *et al*. Universality in Heterogeneous Catalysis. *J. Catal.* **2002**, *209*, 275–278.
52. Ruff, M.; Takehiro, N.; Liu, P.; Norskov, J. K.; Behm, R. J. Size-Specific Chemistry on Bimetallic Surfaces: A Combined Experimental and Theoretical Study. *Chem. Phys. Chem.* **2007**, *8*, 2068–2071.
53. Zhang, J.; Jin, H.; Sullivan, M. B.; Lim, F. H. L.; Wu, P. Study of Pd−Au Bimetallic Catalysts for CO Oxidation Reaction

by DFT Calculations. *Phys. Chem. Chem. Phys.* **2009**, *11*, 1441–1446.
54. Everson, M. P.; Jaklevic, R. C.; Shen, W. Measurement of the Local Density of States on a Metal Surface: Scanning Tunneling Spectroscopy Imaging of Au(111). *J. Vac. Sci. Technol., A* **1990**, *8*, 3662–3665.
55. Crommie, M. F.; Lutz, C. P.; Eigler, D. M. Imaging Standing Waves in a 2-Dimensional Electron-Gas. *Nature* **1993**, *363*, 524–527.
56. Nanayakkara, S. U.; Sykes, E. C. H.; Fernandez-Torres, L. C.; Blake, M. M.; Weiss, P. S. Long-Range Electronic Interactions at a High Temperature: Bromine Adatom Islands on Cu(111). *Phys. Rev. Lett.* **2007**, *98*, 2061081–2061084.
57. Madhavan, V.; Chen, W.; Jamneala, T.; Crommie, M. F.; Wingreen, N. S. Tunneling into a Single Magnetic Atom: Spectroscopic Evidence of the Kondo Resonance. *Science* **1998**, *280*, 567–569.
58. Tierney, H. L.; Baber, A. E.; Sykes, E. C. H. Atomic-Scale Imaging and Electronic Structure Determination of Catalytic Sites on Pd/Cu Near Surface Alloys. *J. Phys. Chem. C* **2009**, *113*, 7246–7250.
59. Suzuki, T.; Hasegawa, Y.; Li, Z. Q.; Ohno, K.; Kawazoe, Y.; Sakurai, T. Electron Standing-Wave Observation in the Pd Overlayer on Au(111) and Cu(111) Surfaces by Scanning Tunneling Microscopy. *Phys. Rev. B* **2001**, *64*, 0814031−0814034.
60. Hasegawa, Y.; Suzuki, T.; Sakurai, T. Modification of Electron Density in Surface States: Standing Wave Observation on Pd Overlayers by STM. *Surf. Sci.* **2002**, *514*, 84–88.
61. Becker, T.; Hövel, H.; Tschudy, M.; Reihl, B. Applications with a New Low-Temperature UHV STM at 5 K. *Appl. Phys. A: Mater. Sci. Process.* **1998**, *66*, S27–S30.